We are IntechOpen,
the world's leading publisher of
Open Access books
Built by scientists, for scientists

6,900
Open access books available

186,000
International authors and editors

200M
Downloads

154
Countries delivered to

Our authors are among the

TOP 1%
most cited scientists

12.2%
Contributors from top 500 universities

CLARIVATE ANALYTICS

BOOK CITATION INDEX

INDEXED

WEB OF SCIENCE™

Selection of our books indexed in the Book Citation Index
in Web of Science™ Core Collection (BKCI)

Interested in publishing with us?
Contact book.department@intechopen.com

Numbers displayed above are based on latest data collected.
For more information visit www.intechopen.com

Silica-Based Nanovectors: From Mother Nature to Biomedical Applications

Monica Terracciano, Luca De Stefano,

Hélder A. Santos, Nicola M. Martucci, Angela Tino,

Immacolata Ruggiero, Ivo Rendina,

Nunzia Migliaccio, Claudia Tortiglione,

Annalisa Lamberti and Ilaria Rea

Additional information is available at the end of the chapter

Abstract

Diatomite is a natural porous silica material of sedimentary origin, formed by remains of diatom skeletons called "frustules." The abundance in many areas of the world and the peculiar physico-chemical properties made diatomite an intriguing material for several applications ranging from food production to pharmaceutics. However, diatomite is a material still rarely used in biomedical applications. In this chapter, the properties of diatom frustules reduced to nanoparticles, with an average diameter less than 350 nm, as potential drug vectors are described. Their biocompatibility, cellular uptake, and capability to transport molecules inside cancer cells are discussed. Preliminary studies of *in vivo* toxicity are also presented.

Keywords: diatomite, porous material, nanovector, bioconjugation, drug delivery

1. Introduction

Nanomedicine is an innovative research field combining nanotechnology and medicine, radically changing the healthcare drug delivery scenario, in particular in the cancer treatment [1]. The application of nanotechnology in the cancer therapy is expected to solve a number of issues associated with conventional therapeutic agents, including lack of targeting capability, nonspecific distribution, systemic toxicity, and low therapeutic index [2, 3].

Nanotechnology has provided the opportunity to get direct access to the cancerous cells selectively with increased drug localization and cellular uptake, making the therapy more patients' compliant, efficient, and painless. Moreover, nano-based systems allow delivery of poor water-soluble molecules (e.g., most of the anticancer drugs) difficult to administer and can also protect the new therapeutics molecules, such as oligonucleotide analogs (e.g., siRNA) from degradation, preserving their therapeutic efficacy while in the blood circulation [3, 4]. Thus, the aim of nanomedicine in cancer therapy is the production of nanoparticles (NPs) able to deliver a drug to a specific site enhancing local drug molecules accumulation and reducing systemic toxicity [5–7]. Different types of organic and inorganic NPs including liposomes, micelles, nanotubes, and porous silicon (PSi) nanostructures have already been investigated for drug delivery purposes [8–13]. In particular, PSi is one of the most inorganic material used in biomedicine due to its unique properties such as high-specific surface area, tunable pores size, biocompatibility, non-toxicity, high loading capability, controllable dissolution kinetic [1, 14, 15]. Moreover, PSi surface can be easily modified using well-known silane and silanol chemistries in order to incorporate gold and magnetic NPs giving to the hybrid complex (i.e., PSi nanocarrier + metallic or magnetic NP) additional diagnostic and therapeutic functions [16].

In recent years, diatomite, a natural porous silica-based material with similar physico-chemical properties to man-made fabricated PSi, has been suggested as feasible alternative to synthetic porous media for biomedical applications [17–20]. Diatomite is a compound of sedimentary origin formed by remains of diatoms deposited on the bottom of seas or lakes [21, 22]. Due to its peculiar properties including highly ordered pore structure, high-specific surface area, modifiable surface chemistry, biocompatibility, non-toxicity, low cost, optical, and photonic properties, diatomite has been used in different applications ranging from optics and photonics to biosensing [23–27]. Despite these properties and the recognition by the Food and Drug Administration (FDA) as Generally Recognized as Safe (GRAS) for foods and pharmaceuticals production, its use in nanomedicine is still surprisingly undervalued [28]. Recently, diatomite has been explored as microcapsules for oral drug delivery resulting in a non-cytotoxic biomaterial with high potential to improve the bioavailability of loaded oral drugs [20]. To date, there is only one manuscript on the intravenous injection of diatomite microparticles into mice, which investigates the biodistribution and tissue damage of this material. This study demonstrated that none of the animals exhibited any observable abnormalities in the major organs after diatomite injections [29]. Over the last few years, diatomite frustules reduced to nanoparticles have been explored as potential nanocarriers for biomedical applications [30, 31].

In this chapter, the properties of diatomite nanoparticles as non-toxic nanocarriers are described. Different surface functionalization strategies performed in order to transport molecules inside cancer cells and to improve diatomite NPs biocompatibility and cellular internalization are summarized. Preliminary studies of *in vivo* toxicity are also reported.

2. Diatomite nanoparticles (DNPs)

Diatomite is a material of sedimentary origin, formed by siliceous skeleton (called "frustule") of diatoms, unicellular microalgae, deposited on the bottom of seas, or lakes over centuries.

Due to the presence of diatom frustules with different size (ranging from 2 μm to 2 mm) and shape, diatomite morphology can be very complicated (**Figure 1**) [32, 33].
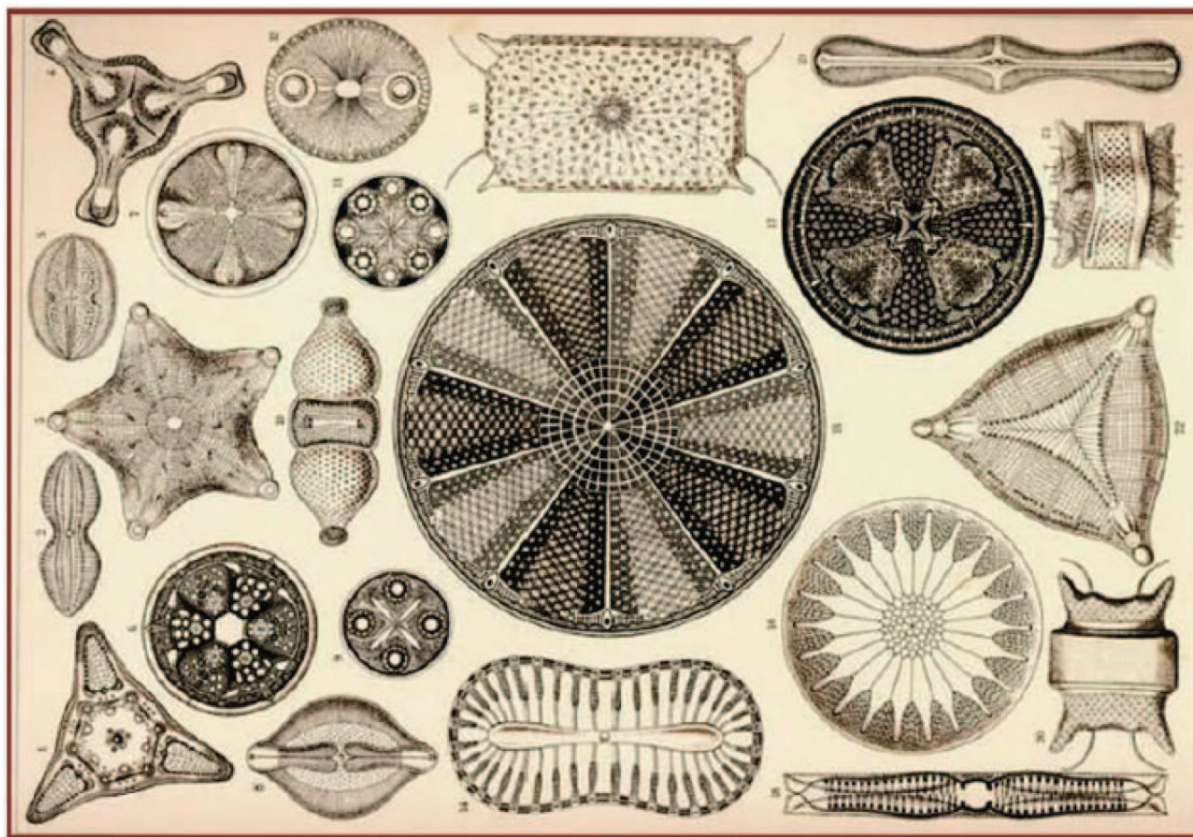

Figure 1. Diatoms by Ernst Haeckel in 'Kunstformen der Natur' 1904 (Reproduced from Ref. [32]).

Diatomite is characterized by highly porous structure with a large specific surface area up to 200 m^2/g [34]. Its fundamental constituent is amorphous silicon dioxide, even if it can contain organic and metallic impurities (e.g., MgO, Al_2O_3, Fe_2O_3) coming from environment [35, 36]. Several processes, including calcination and hot acid treatments, have been developed in order to remove these contaminations from frustules [37, 38].

The abundance in many areas of the world and the peculiar physico-chemical properties (e.g., chemical stability, non-toxicity) made diatomite an intriguing material for several applications ranging from food production to pharmaceutics [39–41].

In recent years, diatom frustules have been investigated as porous platform in several innovative biotechnological applications [42, 43]; the silica surface of diatoms can be easily modified with different functional groups (–SH, –NH₂, –COOH,) for the immobilization of biomolecular probes (DNA, proteins, antibodies) using the reactive silanol (Si–OH) groups present on it [44]. Recent works reported the surface chemical modification of a marine diatom with an antibody used as bioprobe; photoluminescence and fluorescence microscopy were used in order to investigate the antibody-antigen molecular recognition [45, 46]. **Figure 2**

shows an image of marine diatom *Coscinodiscus wailesii* functionalized with an antibody after the interaction with the corresponding rhodamine labeled antigen; the dose-response curve of biosensor (i.e., diatom platform + antibody) is also reported [45].
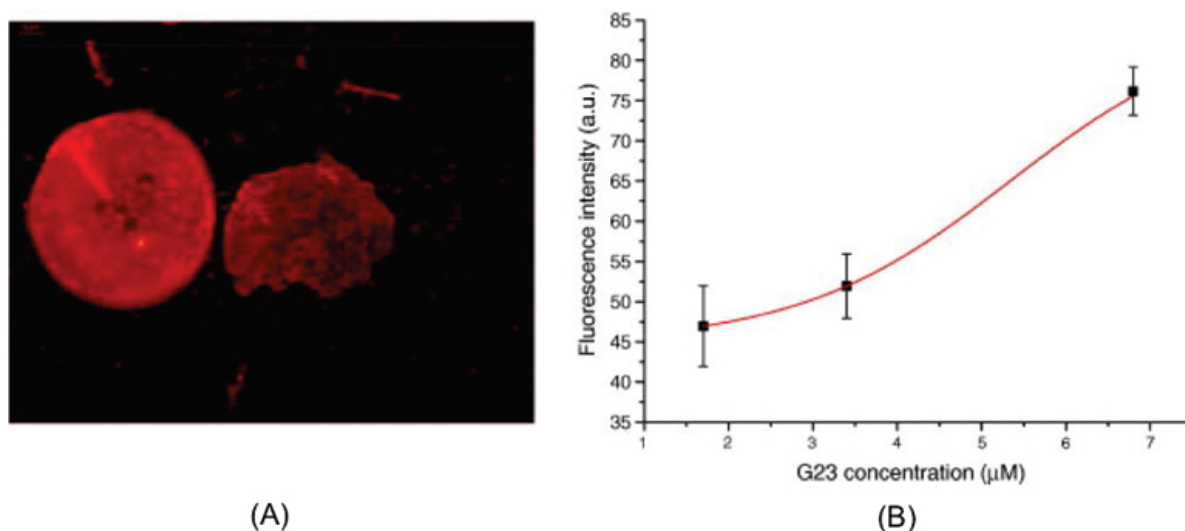

Figure 2. (A) Image of diatom frustules after the interaction between an antibody, covalently linked on them, and the corresponding rhodamine labeled antigen. (B) Fluorescence intensity versus antigen concentration (Reproduced from Ref. [45]).

Although diatomite, produced in tons by mining industry, is a cheaper material compared to diatom frustules, it is still scarcely used in biomedical applications. Recent pioneering papers demonstrated the use of diatomite silica microshells as microcapsules for oral drug delivery [17, 20, 47]. For example, indomethacin, an anti-inflammatory drug poorly soluble in water was explored as model drug in experiments of drug loading and release [18].

More recent works explored the possibility to obtain NPs with a diameter less than 300 nm from micrometric diatomite powder by means of a process based on mechanical crushing, sonication, and filtering [30]. The size reduction is fundamental in drug delivery applications in order to optimize the cellular uptake of particles.

The process for diatomite nanoparticles (DNPs) fabrication is briefly described as follows. About 5 g of diatomite powder was dissolved in 250 ml of absolute ethanol and sonicated for 5 h in order to break up macroscopic aggregates. The dispersion was then filtered through a nylon net filter with pore size of 41 μm (Millipore). In order to remove the organic and inorganic contaminants [34, 36] from natural diatomite, purification treatments were performed: the diatomite dispersion was then centrifuged and the pellet suspended in piranha solution (2 M H_2SO_4, 10% H_2O_2) for 30 min at 80°C. Dispersion was again centrifuged for 30 min at 13,500 rpm, and the supernatant removed. Next, diatomite was washed twice with deionized water. 5.0 M HCl solution was then added to diatomite and incubated over night at 80°C. After HCl incubation, the diatomite dispersion was centrifuged for 30 min and the supernatant removed. The pellet was then washed twice with deionized water in order to remove the excess of HCl.

Micrometric particles

Nanometric particles
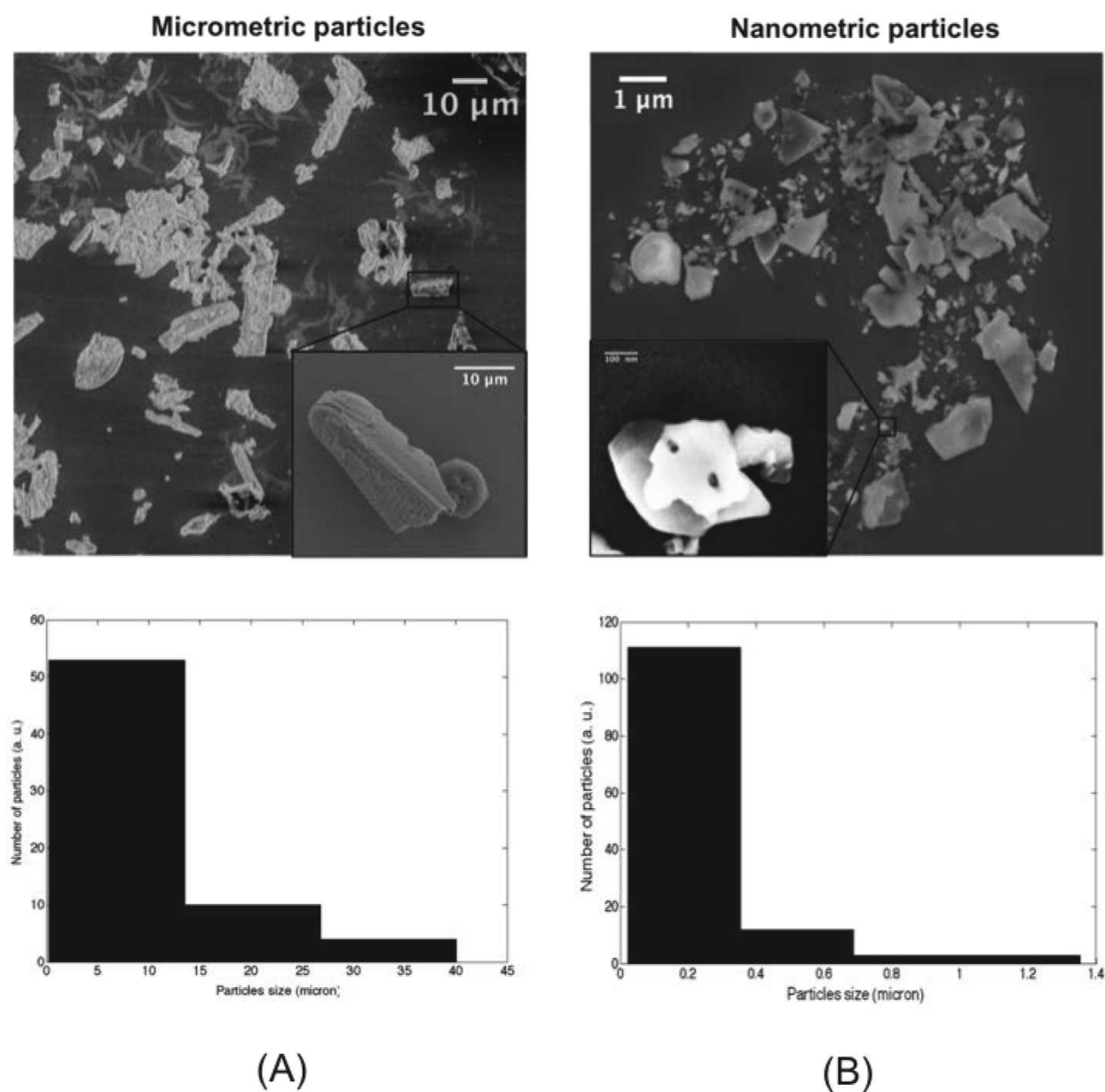
Figure 3. (A) SEM images of diatomite frustules before size reduction treatments and corresponding histogram of particles size distribution. (B) SEM images of diatomite particles after size reduction and corresponding histogram of particles size.

Figure 3 shows the scanning electron microscope (SEM) images of diatomite fragments before (A) and after (B) size reduction. Before treatments, diatomite was composed by fragments with circular, elliptical, elongated, and squared shape. The histogram of particle size showed dimensions distribution ranging from few microns up to about 40 μm with an average maximum size of 7 μm. From these images, it was also possible to appreciate the porous morphology of diatomite useful for drug loading. Morphological characterization, performed after size reduction and purification, revealed the presence of diatomite fragments with different shape and size distribution, ranging from few nanometers to about 1 μm, with an average maximum size of 250 nm. Size of polydispersity can be reduced performing more

filtration steps using filters of 0.45 μm. After nanometric size reduction, it is still possible to observe the porous structure of the NPs with pores of about 40 nm in size.

Dynamic light scattering (DLS) analysis was used in order to investigate size and surface charge of the purified diatomite NPs in water (pH = 7). **Figure 4** shows size and zeta-potential distributions with average values of 220 ± 90 nm and −19 ± 5 mV, respectively. The negative value of zeta potential is due to Si–OH groups present on the surface of DNPs after piranha treatment.
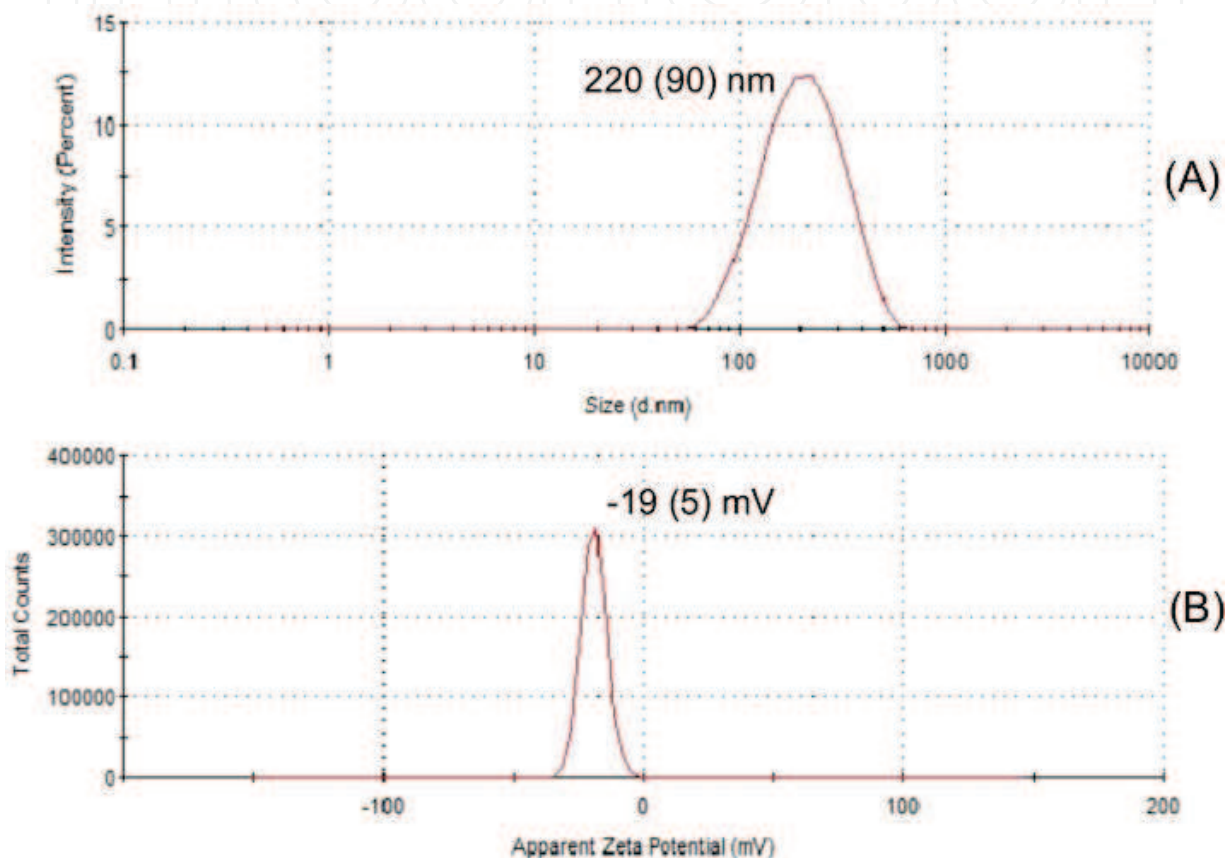
Figure 4. Size (A) and zeta-potential (B) distributions of diatomite nanoparticles in water (pH = 7) (Reproduced from Ref. [30]).

A critical issue for biomedical applications of new drug delivery nanocarriers is the evaluation of their potential toxicity and biocompatibility [17, 48, 49]. *In vitro* cytotoxicity of DNPs can be evaluated by a 3-(4,5-dimethylthiazol-2-yl)-2,5-diphenyltetrazolium bromide (MTT) assay, a method based on the reduction of MTT by cellular oxidoreductases of viable cells that yield the formation of crystalline blue formazan. Human lung epidermoid carcinoma (H1355) cells were used as an *in vitro* cell model to test the cytotoxicity of DNPs. H1355 cells were incubated with different concentrations of diatomite NPs for 24, 48, and 72 h. The obtained results are shown in **Figure 5**. H1355 cells exposed to increasing NP concentrations (20, 100, 200 and 300 μg/ml) show an average viability lower than 100%, demonstrating a very low toxicity of NPs and confirming their potentialities as nanovectors in nanomedicine [50, 51].
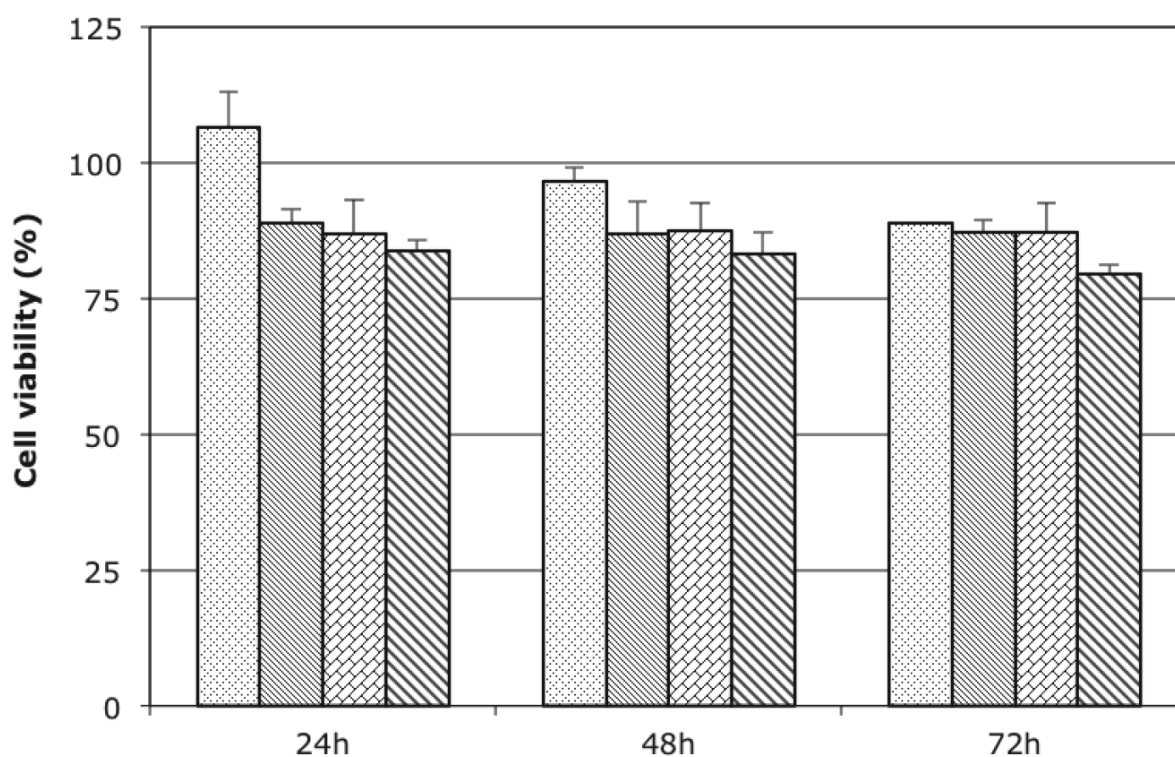
Figure 5. Cytotoxicity assessment of DNPs using MTT assay. Cell viability of H1355 cells treated with 20, 100, 200, and 300 µg/ml of nanoparticles for 24, 48, and 72 h at 37°C. Data represent the mean ± s.d. (n = 3). Cell viability was expressed as the percentage of viable cells compared with cells cultured without NPs as control (100%) (Reproduced from Ref. [31]).

## 3. siRNA delivery by DNPs inside cancer cells

Small interfering ribonucleic acid (siRNA) is a powerful approach for silencing genes associated with a variety of pathologic conditions, but its systemic delivery is inefficient due to the difficulty to penetrate the cell membrane [52, 53]. siRNA conjugation to nanovectors (e.g., liposomes, gold and magnetic NPs, quantum dots) is one of the possible strategies developed to overcome this challenging problem [54, 55]. DNPs have been shown as potential nanocarriers for siRNA transport inside cancer cells and gene expression silencing [31].

siRNA* (labeled with Dy547), complexed with a poly-D-Arg peptide, was loaded onto DNPs following the functionalization procedure sketched in **Figure 6**. Briefly, (3-aminopropyl)triethoxysilane (APTES)-functionalized diatomite reacts with N-(γ -maleimidobutyryloxy) sulfosuccinimide (NHS) ester (sulfo-GMBS), a water-soluble amine-to-sulfhydryl crosslinker that contains NHS-ester and maleimide reactive groups at opposite ends of a short spacer arm that allow covalent conjugation of amine-(diatomite surface) and sulfhydryl-containing molecules (peptide). A poly-arginine peptide and a nonpolar homopeptide, used as negative control, were used in a molar nitrogen/phosphate ratio of 20:1, previously described as optimal condition to form a stable complex with siRNA [31].
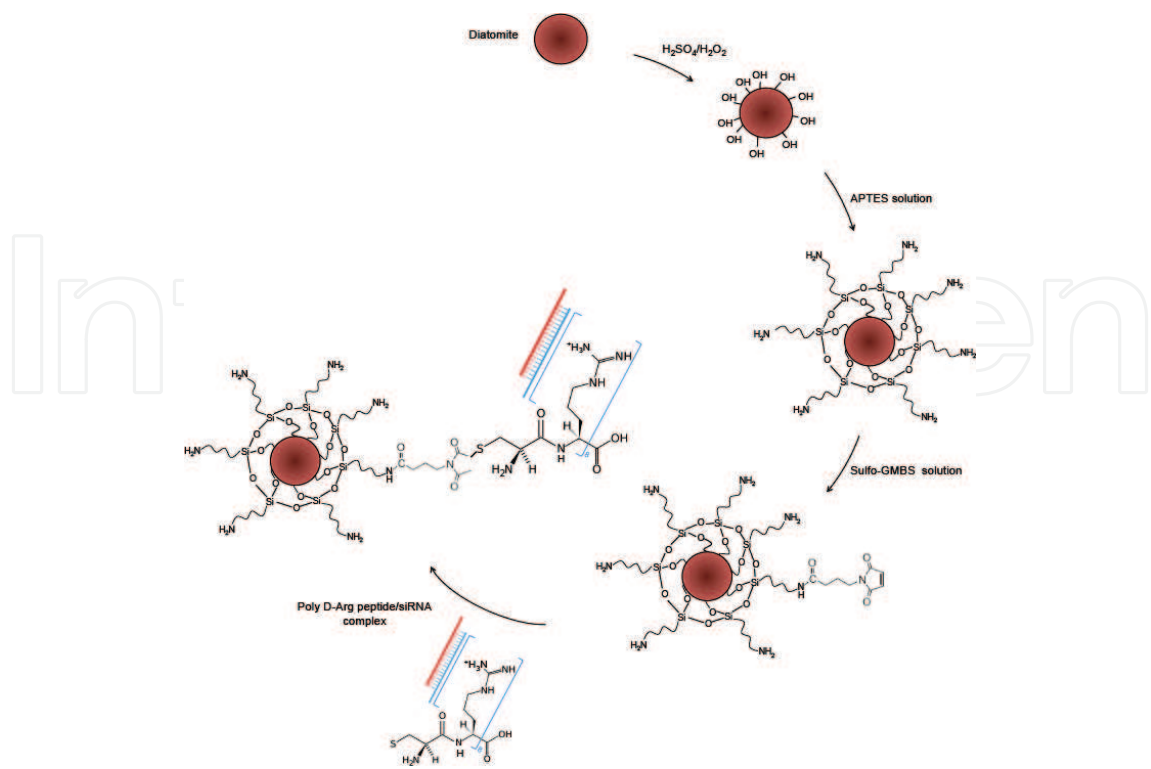
Figure 6. Functionalization scheme of diatomite frustules with labeled siRNA (siRNA*) (Reproduced from Ref. [31]).

In order to study the uptake and intracellular localization of the nanoparticles, H1355 cells (50 × 10³/coverslip) were incubated with 300 μg/ml of siRNA* modified DNPs (DNPs-siRNA*) for 24 h. A representative confocal microscopy acquisition was reported in **Figure 7**.
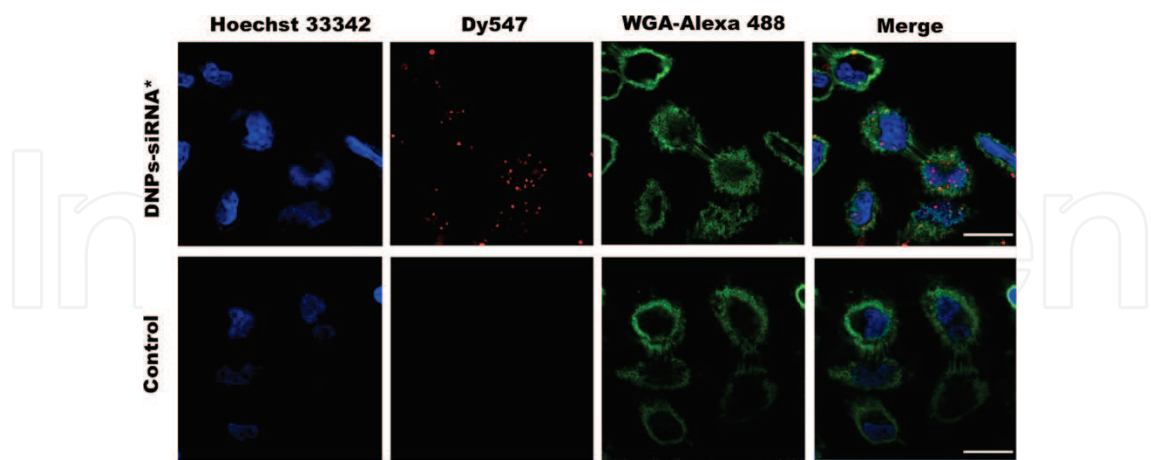

Figure 7. Confocal microscopy on cells treated with siRNA*-modified diatomite nanovectors (first line) and untreated cells as control (second line). Cell nuclei and membranes were stained with Hoechst 33342 and WGA-Alexa Fluor 488, respectively. siRNA was labeled with Dy547. Scale bar corresponds to 20 μm.

Cell nuclei were stained with Hoechst 33342 (blue), whereas WGA-Alexa Fluor 488 (green) and Dy547 (red) were used to stain cell membranes and siRNA, respectively. In **Figure 7**, the

cytoplasmic localization of DNPs-siRNA* is well evident and it was observed as both spots and diffuse signal [56–59]; no red fluorescence was found inside the nuclei. The efficiency of DNPs-siRNA* internalization was quantified by fluorescence microscopy: counting the number of red fluorescent cells and the total number of cells (determined in bright field), a ratio of about 75% was calculated.

The capability of a siRNA direct toward glyceraldehyde 3-phosphate dehydrogenase (GAPDH), conjugated on DNPs, to determine gene knockdown, was evaluated by Western blot analysis; a scramble (SCR) siRNA was used as negative control. A conventional transfection method (Lipofectamine 2000) was carried out to compare the two siRNA uptake systems [31].

The obtained results are showed in **Figure 8**. The densitometric analysis of the bands (Panel B) shows a decrease in the GAPDH protein expression (Panel A, upper gel) of about 22% (lane 2) after 48 h incubation at 37°C with respect to control and DNPs-SCR-siRNA-treated cells (lane 1 and lane 3, respectively). The analysis of GAPDH expression level when lipofectamine was used is reported in panels C and D; a down-regulation of about 20% is observed.
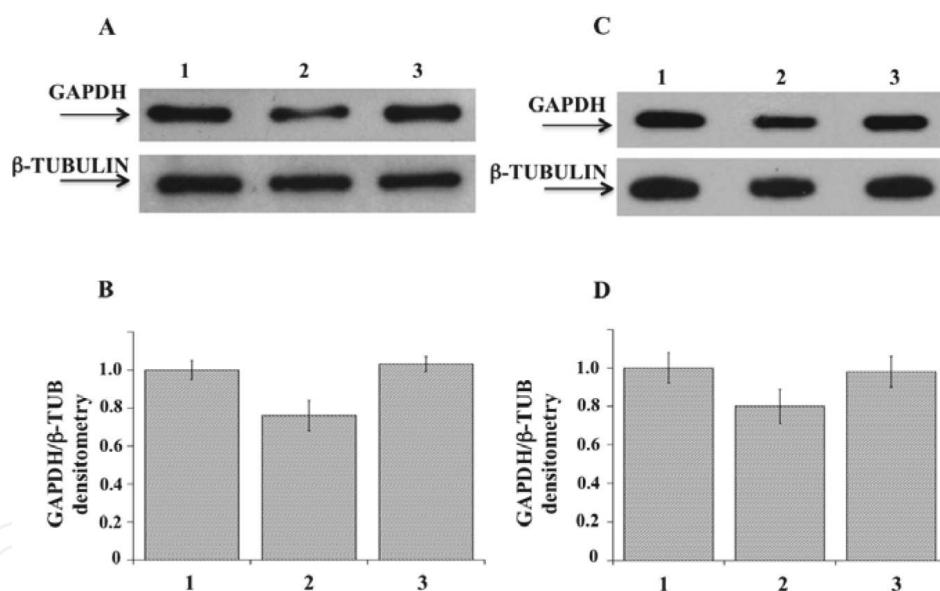

Figure 8. (A) Immunoblotting analysis of GAPDH (upper gel) and β-tubulin (lower gel) protein expression in DNPs-siRNA-treated cells. Lanes: (1) control cells; (2) DNPs-GAPDH-siRNA; (3) DNPs-SCR-siRNA. (B) Densitometric intensity band ratio of GAPDH and β-tubulin used as internal control. The intensities of the bands were expressed in arbitrary units. (C) Immunoblotting analysis of GAPDH (upper gel) and β-tubulin (lower gel) protein expression in lipofectamine-siRNA transfected cells. Lanes: (1) control cells; (2) GAPDH-siRNA; (3) SCR-siRNA. (D) Densitometric intensity band ratio of GAPDH and β-tubulin used as internal control. The intensities of bands were expressed in arbitrary units. Each measurement and Western blot were carried out in triplicate. Error bars indicate the maximum deviation from the mean value of two independent experiments (Reproduced from Ref. [31]).

Nevertheless, the decrease in the protein expression obtained with the two delivery methods was comparable; the use of diatomite as nanovectors allows high stability, biocompatibility, biodegradability, together with high payloads of drugs, selective cell targeting, co-delivery of

molecules functioning with a different mechanism of action (e.g., drugs and siRNA) and controlled release of active compounds at the molecular level.

4. Dual-biofunctionalization of DNPs for enhanced stability, biocompatibility, and cellular internalization in cancer cells

The small size, appropriate aqueous solution stability, biocompatibility, and cellular uptake are the most important characteristics of NPs as drug delivery systems. The PEGylation [i.e., the covalent attachment of poly(ethylene glycol)] of NPs has been frequently used in the design of drug nanocarriers, as a valid functionalization to improve physico-chemical properties of NPs such as the increase of their stability in aqueous medium reducing the nonspecific aggregation and improving biocompatibility, drug loading, and cellular internalization [60–62]. Moreover, an efficient approach to improve the NPs' cellular uptake is to bind them to peptides that can cross the cellular membranes, enhancing their translocation inside the cells [63]. A valid strategy to improve the intracellular drug delivery of nanocarriers is their bioconjugation with cell-penetrating peptide (CPP), due to the CPP property to overcome the
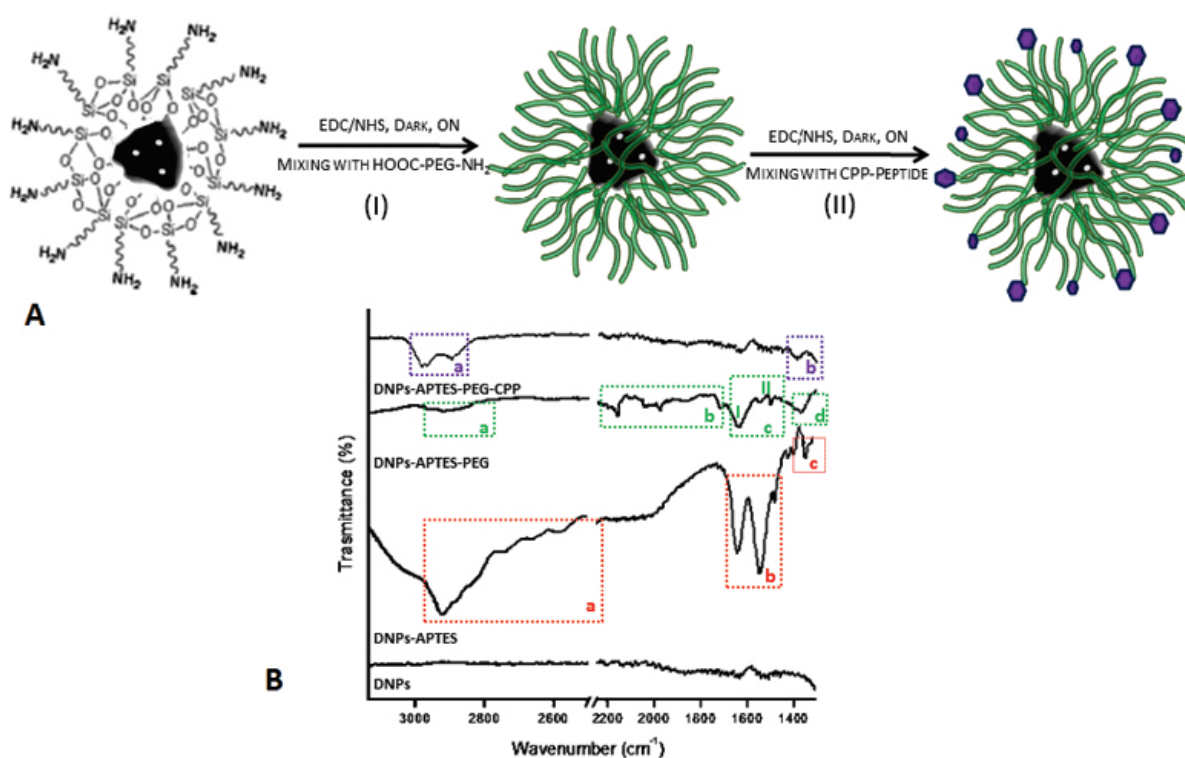

Figure 9. (A) Schematic representation of the DNPs functionalization. Reaction I, the PEGylation of DNPs-APT (I) via EDC/NHS, under stirring overnight (ON) at room temperature. Reaction II, CPP-peptide bioconjugation of DNPs-APT-PEG via EDC/NHS, under stirring ON at room temperature. (B) ATR-FTIR spectra of DNPs before the biofunctionalization, after the silanization process, after the PEGylation, and also after the CPP-peptide bioconjugation. The **a** indicates CH_x stretching vibration, **b** the bending mode of the free NH_2, **c** the C–N stretching, **d** the C–H bending vibrations, and **c-I** and **c-II** N–H bending vibration, and the C–N stretching vibration, respectively.

lipophilic barrier of the cellular membranes and deliver NPs inside the cells [64, 65]. PEGyla-tion and CPP bioconjugation have been used as biofunctionalization strategies to improve the physico-chemical and biological properties of the DNPs, in order to enhance the intracellular uptake in cancer cells and to increase the biocompatibility of APTES modified-DNPs (DNPs-APT) [66]. The decoration of NPs' surface with PEG chains was achieved via covalent bond between the carboxyl groups (–COOH) of PEG molecules and the amino groups (–NH_2) of silanized DNPs using 1-ethyl-3-(3-dimethylaminopropyl)carbodiimide (EDC)/NHS chemistry (**Figure 9A, I**) [30, 31]. Subsequently, the free amino groups of DNPs-APT-PEG were chemi-cally conjugated with the carboxyl groups of CPP, by EDC/NHS chemistry (**Figure 9A, II**) [67].

The improvement of the NPs' stability in aqueous solutions was confirmed by hydrodynamic diameter, PDI, and surface charge ζ-potential measurements, before and after the DNPs' surface modification. A progressive decrease of the nano-aggregates size from 364 ± 3 nm (DNPs-APT) to 346 ± 4 nm after PEGylation (DNPs-APT-PEG), and to 340 ± 8 nm after CPP-conjugation (DNPs-APT-PEG-CPP), was observed. This result is due to an increase of the DNPs surface repulsion forces of the modified surface (DNPs-bare,−19.2 ± 2.0 mV; DNPs-APT, +19.8 ± 3.0 mV; DNPs-APT-PEG, +35.6 ± 1.5 mV; DNPs-APT-PEG-CPP, +40 ± 2 mV), which can be attributed to the positive charge of PEG-peptide and CPP onto the NPs' surface. The result of DNPs modification was also evaluated by attenuated total reflectance Fourier transform infrared spectroscopy (ATR–FTIR). **Figure 9B** shows the progressive change of DNPs FTIR spectra after each modification step. After the silanization process, the DNPs-APT displayed the typical bands of APTES corresponded to the CH_x stretching at 2941–2570 cm^{-1}, the free NH_2 bending mode at 1630–1470 cm^{-1}, and the C–N stretching at 1385 cm^{-1} [68, 69]. After the PEGylation, the DNPs-APT-PEG showed the stretching bands of the CH_x at 2960–2849 cm^{-1}, the C–H bending vibrations at 2160–1722 cm^{-1}, the amide I band at 1640 cm^{-1} associated with the C=O stretching vibration, the amide II resulted from the N–H bending vibration, and the C–N stretching vibration at 1580 and 1360 cm^{-1}, respectively, thus confirming the covalent binding of the PEG molecules onto the NPs' surface [69]. After incubation with the CPP-peptide, the DNPs-APT-PEG-CPP displayed a band of the CH_x stretching at 2984–2881 cm^{-1}, and the C–N stretching of amide II at 1930 cm^{-1}, confirming the successful of CPP-peptide bioconjugation onto DNPs surface [69, 70].

The hemocompatibility of NPs is of critical importance for their systemic administration as drug delivery systems, in order to avoid serious risks to human health [71, 72]. The effect of modified-DNPs on red blood cells (RBCs) was evaluated studing the % lysed RBCs and their morphology after exposure to the NPs at increasing incubation times (1, 4, 24, 34 and 48 h) and concentrations (25, 50, 100, and 200 μg/ml) [66, 73]. The NPs hemotoxicity was qualitatively determined by naked-eye color evaluation of RBCs' supernatant incubated with modified-DNPs, observing an higher hemotoxicity degree of the DNPs-APT than PEG and CPP modified-DNPs, since the red color intensity of DNPs-APT-RBCs supernatant was closer to the positive control one (water), as shown in **Figure 10A**. The %-hemolysis determined by spectrophotometric analysis of the supernatants after 48 h incubation at the maximum concentration of modified-DNPs (200 μg/mL) was 34% for DNP-APT, 7% for DNP-PEG, and

1.3% for CPP-DNP, demonstrating that the dual-biofunctionalization improved the DNPs hemocompatibility (**Figure 10B**).
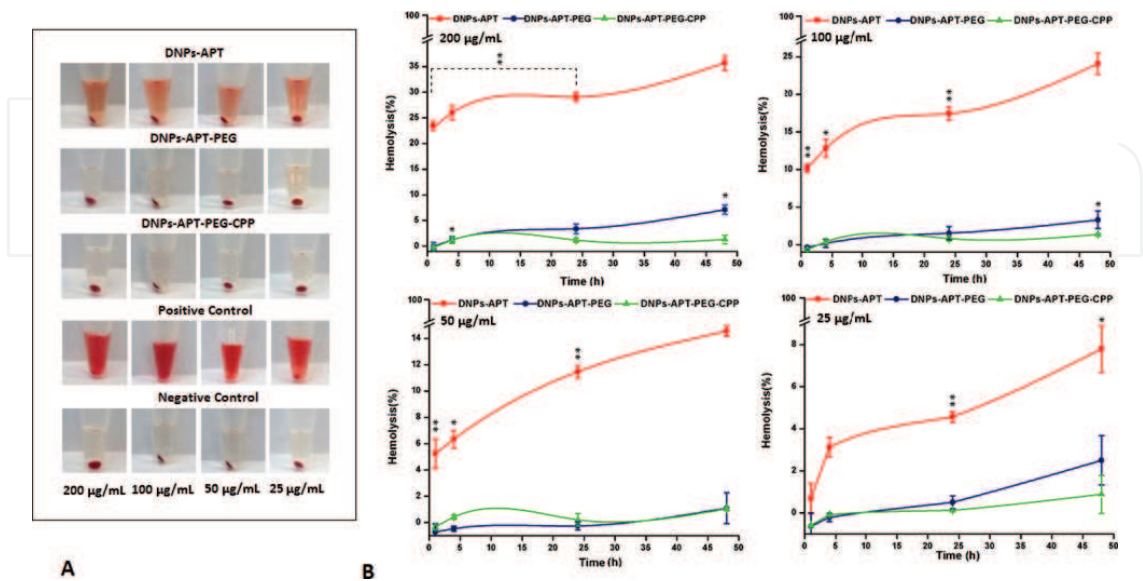

Figure 10. (A) Representative pictures of the RBCs after interaction with the modified-DNPs. The DNPs were incubated with the cells for 48 h and at different concentrations (25, 50, 100, and 200 μg/ml). (B) Hemotoxicity of APT-, PEG-, and CPP-modified DNPs incubated for 48 h at different concentrations (25, 50, 100, and 200 μg/ml) with RBCs, estimated by spectrophotometric methods (577 nm) to analyze the amount of lysed-hemoglobin in the supernatants. The level of significance from negative control was set as probabilities of *$p < 0.05$, **$p < 0.01$, and ***$p < 0.001$ by ANOVA. Error bars represent s.d. ($n = 3$).
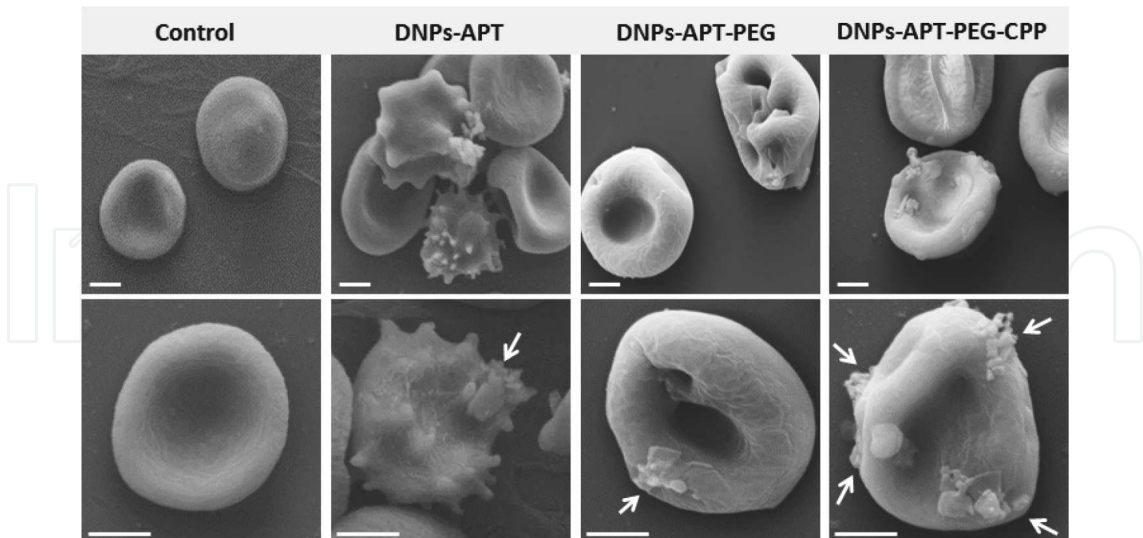
Figure 11. SEM pictures of the RBCs morphological modification after the exposure to the modified DNPs. The modified DNPs (100 μg/ml) were incubated with RBCs for 4 h at room temperature. The DNPs-APT showed the higher toxicity than the PEG and CPP-modified DNPs, resulting in severe morphological changes of cell. The CPP-bioconjugation improved significantly the DNPs–cells membrane interactions, as indicated by white arrows. Scale bars are 3 μm (Reproduced from Ref. [66] with permission from the Royal Society of Chemistry).

Figure 11 shows SEM characterization of RBCs after exposure to the modified-DNPs (200 μg/ml for 4 h at room temperature). The RBCs, in the presence of DNP-APT completely altered their morphology, changing from the biconcave-like disks to shrinked shape, with consequent hemolysis due to the free positive amine groups on the surface of the NPs, which strongly interact with the negative charge surface of the RBCs. In the case of PEGylated particles, there was a slight change in the RBC's morphology by membrane wrapping around with the appearance of small holes, but without significant hemolysis. The relevant decrease of the DNPs-APT hemotoxicity after PEGylation is due to the improved biocompatibility of the NPs as a result of PEGylation [74, 75]. In the case of DNPs-APT-PEG-CPP, there were no relevant changes observed in the morphology due to the low cytotoxicity of CPP-peptide, which improved the DNPs' biocompatibility [76–78].

Efficient delivery of the nanocarriers to the cells and tissues is another key requirement for drug delivery applications. The CPP-peptide, used to improve the cellular uptake of the DNPs, is a short cationic peptide with intrinsic ability to enter cells and mediate uptake of a wide range of molecular cargos, such as oligonucleotides, small molecules, siRNA, NPs, peptides, and proteins [79–81].
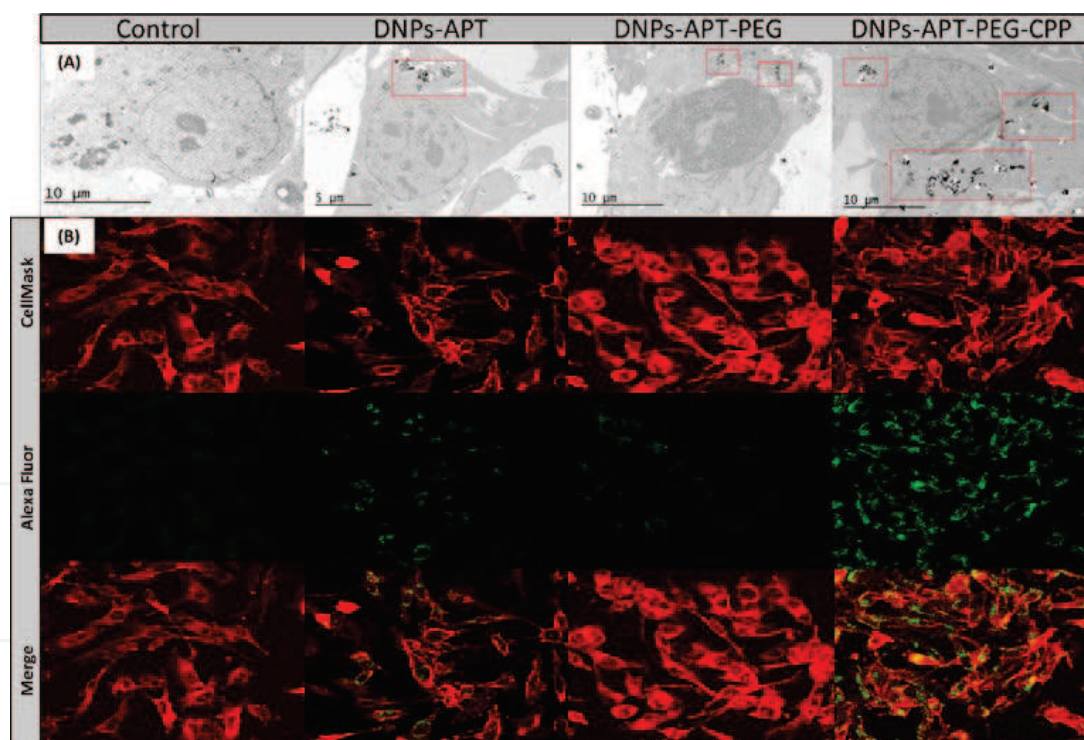
Figure 12. (A) TEM images of MDA-MB-231 cells treated with 50 μg/ml of DNPs-APT, DNPs-APT-PEG, and DNPs-APT-PEG-CPP for 12 h at 37°C. A very small amount of APTES- and PEG-modified DNPs (in dotted boxes) was found inside the cells. In the case of DNPs-APT-PEG-CPP (in dotted boxes), a considerable amount of the NPs was observed inside the cells. Scale bars are 10 μm. (B) Confocal fluorescence microscopy MDA-MB-231 cells treated with 50 μg/ml of APT, APT-PEG, APT-PEG-CPP modified-DNPs for 12 h at 37°C. CellMask® (red) and Alexa Fluor-488® (green) were used to label the cells membrane and the DNPs, respectively. The merge figures are obtained by overlapping the DNPs and the cells membrane images, allowing to determine whether the NPs are located outside (green color) or inside (yellow color) the cells.

The cellular uptake of modified DNPs was evaluated by transmission electron microscope (TEM), after the incubation of MDA-MB 231 breast cancer cells with the NPs (50 µg/mL) for 12 h. In **Figure 12A**, the APTES-modified DNPs were mainly localized in the proximity of the cell membrane, while in the case of the DNPs-APT-PEG, any significant cellular uptake was observed. For the CPP-modified NPs, a considerable amount of DNPs was internalized into the cells with a homogeneous distribution into the cytoplasm and very close to the nucleus. The cellular uptake was also evaluated by confocal fluorescence microscope after DNPs and cellular membrane labeling with Alexa Fluor-488® and CellMask™ Deep Red, respectively (**Figure 12B**). In merged images, for DNPs-APT, the green color is indicative of the presence of DNPs on the cell membrane surface; while for the CPP modified-DNPs, the yellow color, resulting from the co-localization of the green labeled-DNPs and red-stained cancer cell membranes, is representative of NPs located inside the cells. These results confirmed that the CPP bioconjugation is a valid functionalization strategy to increase the cell penetration of DNPs [82, 83].

5. *In vivo* evaluation of DNPs toxicity

In vitro testing is the most common scientific analysis used to determine the effects of NPs toxicity. However, the success of *in vitro* assays is not predictive for promising *in vivo* results; for this reason, *in vivo* evaluation of NPs toxicity is a crucial issue in order to develop safe nanodevices for biomedical applications.

In this context, *Hydra vulgaris* (Cnidaria, Hydrozoa) was used as preliminary *in vivo* model to evaluate diatomite NPs toxicity.

Hydra is a simple multicellular organism at the base of the metazoan evolution. It consists of a tube which is made of two connected epithelial cell layers: the outer ectoderm and inner endoderm, separated by an acellular mesoglea layer (**Figure 13**) [84]. As shown in **Figure 13**, at the top end of the tube, there is the hypostome composed by a mouth surrounded by 6–8 tentacles that contain the most part of stinging cells (cnidocytes or nematocytes) that let *Hydra* to catch its prey [85]. Hydra column has four distinctive sections: the gastric region located between the tentacles and the first (apical) bud; the budding section, which produces the buds; the peduncle, which is located between the lowest bud and basal disc; and the basal disc, which is the foot-like formation [86]. This structural complexity, simpler than vertebrates with central nervous system and specialized organs, but more complex than cultured cells, makes *Hydra* comparable to a living tissue whose cells and distant regions are physiologically connected. It possesses a simple nervous system consisting of a diffuse nerve net throughout the body [87]. *Hydra* typically reproduces asexually resulting in the rapid production of a large number of new organisms that can be cultured in a short period of time. *Hydra* is sensitive to a range of pollutants and has been used as a biological indicator of water pollution [88]. Metal pollutants such as copper, cadmium, and zinc have been tested against different Hydra species, and the relative toxicity based on the median lethal concentration (LC50) for all species was ranked from copper, the most toxic, to cadmium with zinc, the least toxic [88].
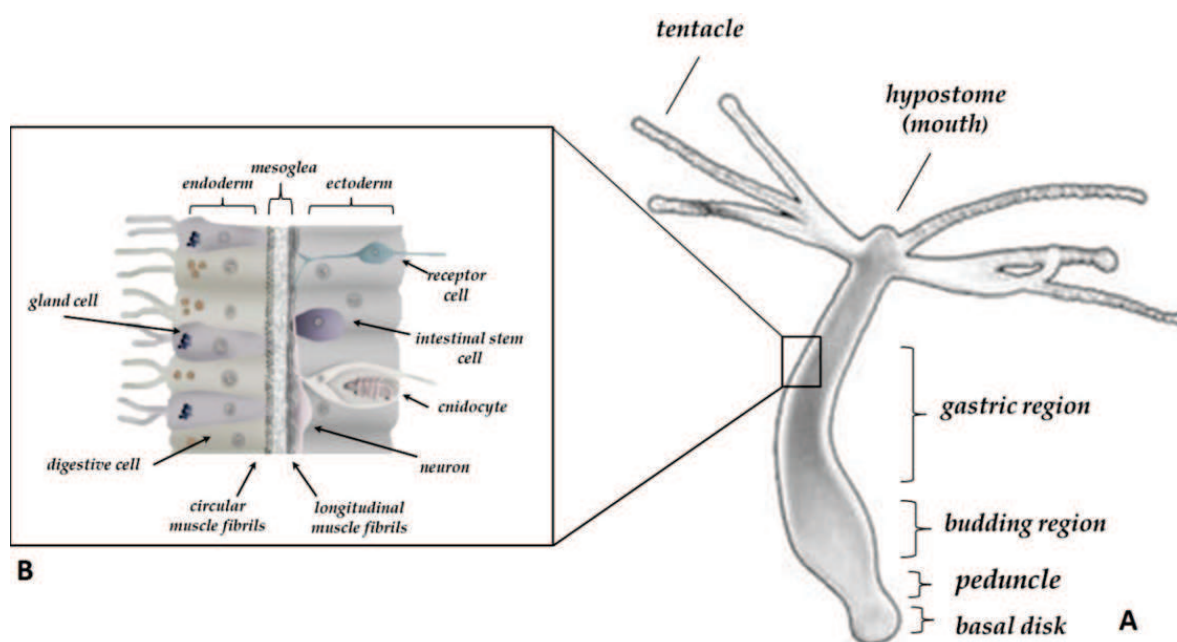
Figure 13. Anatomical structure of *Hydra vulgaris*. The inset shows the bilayer structure characterizing the whole body, from the foot to the tentacles, that is, the ectoderm and endoderm layers separated by the mesoglea. The few specialized cell types differentiated by the interstitial stem cells are shown (neurons, cnidocyte, gland cells).

Hydra has also been used as alternative *in vivo* model, to study the toxicity of different NPs, as well as their uptake and fate [89–91]. Due to a simple tubular body and being diploblastic, an even exposure of the whole animal to NPs by simple soaking is allowed [92, 93]. Several bioassays are available to assess the toxicity of a given substance in terms of acute or sub-lethal toxicity [94]. *Hydra* exposure to different substances may cause alteration of (1) morphological traits and developmental programs, (2) regeneration or pattern formation, and (3) population growth rates.

Toxicity of a substance is conventionally measured in *Hydra* observing changes in the animal morphology following Wilby's classification ranging from score 10 (normal, elongated tentacles and body), 8 (clubbed or bulged tentacles), 6 (shortened tentacles), 5 (tulip phase), 2 (loss of osmoregulation), to 0 (disintegrated) [95]. Scores 10–6 are reversible, sub-lethal indicators, while the tulip phase (score 5 and below) is considered irreversible and used as the endpoint for lethality [92, 95].

Toxicity of diatomite NPs in *Hydra* was investigated monitoring changes in its morphology after exposure to DNPs at increasing incubation times (24, 48 and 72 h) and concentrations (0.5, 1, 1.5, 2.5, 3, 3.5, and 4 mg/mL). *Hydra vulgaris* was asexually cultured in physiological solution by the method of Loomis and Lenhoff with minor modifications [96]. The animals were kept at 18°C and fed three times per week with freshly hatched *Artemia salina* nauplii. All animals were starved 24 h prior to the experiments. For each DNPs concentration, twenty polyps were used [97]. Either control or treated animals were placed into plastic multiwells refreshing the medium every 24 h. The morphophysiological effects of DNPs on *Hydra* were recorded by microscopic examination of each polyp and used to extrapolate the Wilby's score

key. A representative *in vivo* image of *Hydra* after exposure to DNPs is reported in **Figure 14**. Any change in polyp morphology was not observed after exposure to DNP concentrations up 4 mg/mL for 72 h; this result corresponds to score 10 of Wilby's classification.

Figure 14. *In vivo* imaging of Hydra polyps treated with DNPs. Polyp morphology is not affected by the nanoparticle treatment. Scale bar: 1 mm.

These data confirm *in vitro* toxicity results. The transparency of *Hydra* epithelium makes it possible to track and localize fluorescent nanoparticles in the animal body [92–94]. The internalization of DNPs in *Hydra* was evaluated by *in vivo* fluorescence microscopy analysis, after labeling DNPs by Alexa Fluor-488® (DNPs*). Ten living *Hydra* were treated with DNPs* (3.5 mg/mL) up to 72 h. Bright-field and fluorescence images of *Hydra* polyps treated with DNPs* for 24 (C, D) and 72 h (E, F) are reported in **Figure 15**; **Figure 15A, B** shows an untreated animal as control. In all figures, the foot is on the lower part of the panel, while a crown of tentacles surrounds the mouth. The image taken after 24 h (D) shows an intense fluorescence of DNPs, distributed in the whole body and confined to the outer ectoderm. After 72 h (F) of incubation, the DNPs were mainly localized in the inner endodermal cells, due to inter-epithelial migration of free or cell-containing nanoparticles between the two cell layers [92]. These preliminary *in vivo* results are in agreement with the *in vitro* data, confirming that DNPs could be used as safe and biocompatible nanocarrier for long incubation times and up to high concentrations.
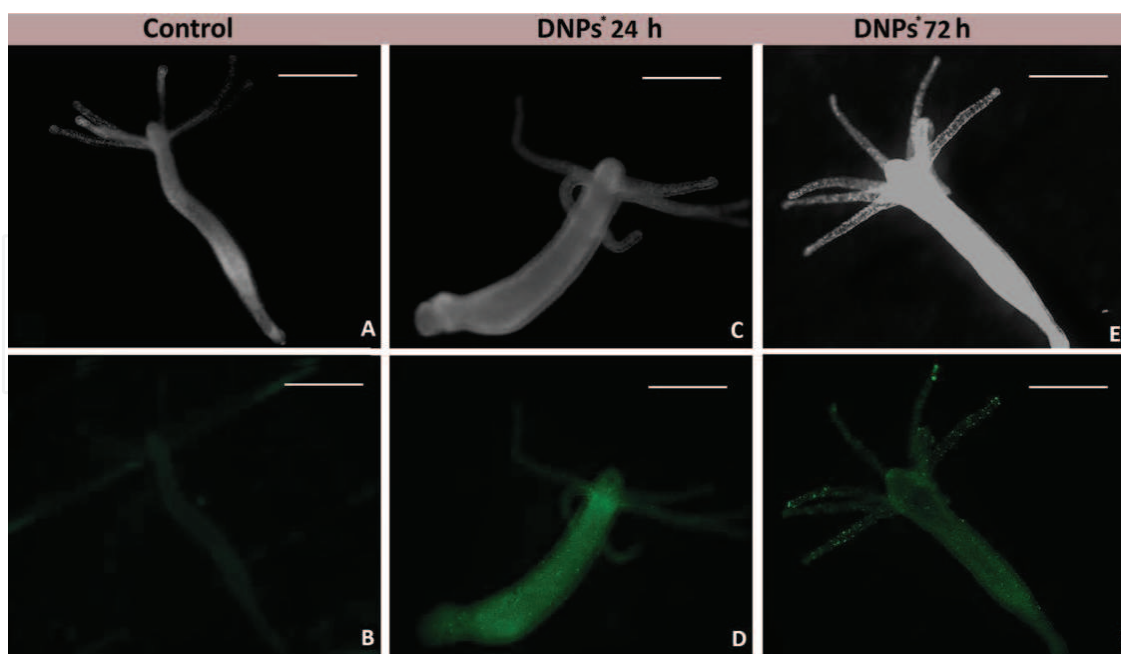
Figure 15. *In vivo* fluorescence imaging of Hydra polyps treated with labeled DNPs (3.5 mg/mL) for different incubation times. Scale bars: 1 mm. The fluorescence pattern appears as rather uniform after 24 h of incubation, while at 72 h it appears as granulates covering most of body regions. They might represent storage vacuoles, as it has been shown for other fluorescent nanoparticles [92, 94].

6. Conclusions and future trends

Diatomite is a fossil material of sedimentary origin formed over centuries by siliceous skeleton of aquatic unicellular microalgae diatoms, with similar physico-chemical properties of man-made fabricated PSi. Due to its ordered pore structure, high surface area, tailorable surface chemistry, high permeability, biocompatibility, non-toxicity, low cost, optical, and photonic properties, diatomite has been exploited as an innovative platform in several biotechnological applications, resulting as a viable and promising cheap alternative to synthetic porous silica. In this chapter, the potentialities of DNPs, with an average size of about 350 nm, as drug nanocarriers were discussed. Preliminary tests of cytotoxicity and cellular uptake demonstrated the biocompatibility of the DNPs and their capability to penetrate inside cancer cells. Different functionalization procedures of diatomite surface for preparation of bioengineered nanovectors were also described. These results, compared with those reported in literature on standard systems, encourage the use of diatomite-based materials as new class of nanostructured drug carriers.

Acknowledgements

Author details

Monica Terracciano[1,2,3], Luca De Stefano[1], Hélder A. Santos[3], Nicola M. Martucci[4], Angela Tino[5], Immacolata Ruggiero[4], Ivo Rendina[1], Nunzia Migliaccio[4], Claudia Tortiglione[5], Annalisa Lamberti[4] and Ilaria Rea[1*]

*Address all correspondence to: ilaria.rea@na.imm.cnr.it

1 Institute for Microelectronics and Microsystems, National Research Council, Naples, Italy

2 Department of Pharmacy, University of Naples Federico II, Naples, Italy

3 Division of Pharmaceutical Chemistry and Technology, Faculty of Pharmacy, University of Helsinki, Helsinki, Finland

4 Department of Molecular Medicine and Medical Biotechnology, University of Naples Federico II, Naples, Italy

5 Institute of Applied Sciences and Intelligent Systems, National Research Council, Naples, Italy

References

[1] M. Ferrari, Cancer nanotechnology: opportunities and challenges. *Nat. Rev. Cancer*, 2005, 5, 161–171.

[2] O. C. Farokhzad and R. Langer, Impact of Nanotechnology on Drug Delivery. *ACS Nano*, 2009, 3, 16–20.

[3] P. Parhi, C. Mohanty and S. K. Sahoo, Nanotechnology-based combinational drug delivery: an emerging approach for cancer therapy. *Drug Discov. Today*, 2012, 17, 1044–1052.

[4] R. van der Meel, L. J. Vehmeijer, R. J. Kok, G. Storm and E. V. van Gaal, Ligand-targeted particulate nanomedicines undergoing clinical evaluation: current status. *Adv. Drug Deliv. Rev.*, 2013, 65, 1284–1298.

[5] J. Shi, A. R. Votruba, O. C. Farokhzad, R. Langer, Nanotechnology in Drug Delivery and Tissue Engineering: From Discovery to Applications. *Nano Lett.*, 2010, 10, 3223–3230.

[6] S. M. Moghimi, A. C. Hunter and J. C. Murray, Nanomedicine: current status and future prospects. *FASEB J.*, 2015, 19, 311–330.

[7] M. Ding, N. Song, X. He, J. Li, L. Zhou, H. Tan, Q. Fu and Q. Gu, Toward the Next-Generation Nanomedicines: Design of Multifunctional Multiblock Polyurethanes for Effective Cancer Treatment. *ACS Nano*, 2013, 7, 1918–1928.

[8] V. P. Torchilin, Recent advances with liposomes as pharmaceutical carriers. *Nat. Rev. Drug Discov.*, 2005, 4, 145–160.

[9] H. A. Santos (Ed), Porous Silicon for Biomedical Applications 1st Edition, Elsevier, 2014.

[10] M. J. Sailor and J. H. Park, Hybrid nanoparticles for detection and treatment of cancer. *Adv. Mater.*, 2012, 24, 3779–3802.

[11] B. Herranz-Blanco, D. Liu, E. Mäkilä, M. A. Shahbazi, E. Ginestar, H. Zhang, V. Aseyev, V. Balasubramanian, J. Salonen, J. Hirvonen and H. A. Santos, On-Chip Self-Assembly of a Smart Hybrid Nanocomposite for Antitumoral Applications. *Adv. Funct. Mater.*, 2015, 25, 1488–1497.

[12] L. M. Bimbo, L. Peltonen, J. Hirvonen and H. A. Santos, Toxicological profile of therapeutic nanodelivery systems. *Curr. Drug Metab.*, 2012, 13, 1068–1086.

[13] L. Russo, F. Colangelo, R. Cioffi, I. Rea and L. De Stefano, A Mechanochemical Approach to Porous Silicon Nanoparticles Fabrication. *Materials*, 2011, 4, 1023–1033.

[14] F. Muhammad, M. Guo, W. Qi, F. Sun, A. Wang, Y. Guo, and G. Zhu, pH-Triggered Controlled Drug Release from Mesoporous Silica Nanoparticles via Intracelluar Dissolution of ZnO Nanolids. *J. Am. Chem. Soc.*, 2011, 133, 8778–8781.

[15] Y. Zhao, B. G. Trewyn, I. Slowing and V. S. Lin, Mesoporous silica nanoparticle-based double drug delivery system for glucose-responsive controlled release of insulin and cyclic AMP. *J. Am. Chem. Soc.*, 2009, 131, 8398–8400.

[16] L. Gu, D. J. Hall, Z. Qin, E. Anglin, J. Joo, D. J. Mooney and M. J. Sailor, In vivo time-gated fluorescence imaging with biodegradable luminescent porous silicon nanoparticles. *Nat. Commun.*, 2013, 4, 2326.

[17] D. Losic, J. G. Mitchell and N. H. Voelcker, Diatomaceous Lessons in Nanotechnology and Advanced Materials. *Adv. Mater.*, 2009, 21, 2947–2958.

[18] M. S. Aw, S. Simovic, Y. Yu, J. Addai-Mensah and D. Losic, Porous silica microshells from diatoms as biocarrier for drug delivery applications. *Powder Technol.*, 2012, 223, 52–58.

[19] M. Sumper and E. Brunner, Learning from Diatoms: Nature's Tools for the Production of Nanostructured Silica. *Adv. Funct. Mater* ., 2006, 16, 17–26.

[20] H. Zhang, M. A. Shahbazi, E. Mäkilä, T. H. da Silva, R. L. Reis, J. Salonen, J. T. Hirvonen and H. A. Santos, Diatom silica microparticles for sustained release and permeation enhancement following oral delivery of prednisone and mesalamine. *Biomaterials*, 2013, 34, 9210–9219.

[21] M. A. Ferrara, P. Dardano, L. De Stefano, I. Rea, G. Coppola, I. Rendina, R. Congestri, A. Antonucci, M. De Stefano and E. De Tommasi, Optical Properties of Diatom Nanostructured Biosilica in Arachnoidiscus sp: Micro-Optics from Mother Nature. *Plos One*, 2014, 9, 103750.

[22] L. De Stefano, I. Rendina, M. De Stefano, A. Bismuto and P. Maddalena, Marine diatoms as optical chemical sensors. *Appl. Phys. Lett.*, 2005, 87, 233902.

[23] J. Parkinson and R. Gordon, Beyond micromachining: the potential of diatoms. *Trends Biotechnol.*, 1999, 17, 230–232.

[24] T. Fuhrmann, S. Landwehr, M. El Rharbi-Kucki and M. Sumper, Diatoms as living photonic crystals. *Appl. Phys. B*, 2004, 78, 257–260.

[25] P.J. Lopez, J. Desclés, A.E. Allen, C. Bowler, Prospects in diatom research. *Curr Opin Biotechnol*. 2006, 16, 180-186.

[26] S. Lettieri, A. Setaro, L. De Stefano, M. De Stefano and P. Maddalena, The Gas-Detection Properties of Light-Emitting Diatoms. *Adv. Funct. Mater.*, 2008, 18, 1257–1264.

[27] F. Xu, Y. Wang, X. Wang, Y Zhang, Y. Tang and P. Yang, A Novel Hierarchical Nanozeolite Composite as Sorbent for Protein Separation in Immobilized Metal-Ion Affinity Chromatography. *Adv. Mater.*, 2003, 15, 1751–1753.

[28] IARC MONOGRAPHS ON THE EVALUATION OF CARCINOGENIC RISKS TO HUMANS Volume 68 (1997) Silica, Some Silicates, Coal Dust and para-Aramid Fibrils.

[29] B. Delalat, V.C. Sheppard, S.R. Ghaemi, S. Rao, C.A. Prestidge, G. McPhee, M.L. Rogers, J.F. Donoghue, V. Pillay, T.G. Johns, N. Kröger, N.H. Voelcker, Targeted drug delivery using genetically engineered diatom biosilica. *Nat. Commun.*, 2015, 6, 8791.

[30] I. Ruggiero, M. Terracciano, N. M. Martucci, L. De Stefano, N. Migliaccio, R. Taté, I. Rendina, P. Arcari, A. Lamberti and I. Rea, Diatomite silica nanoparticles for drug delivery. *Nanoscale Res. Lett.*, 2014, 9, 1–7.

[31] I. Rea, N. M. Martucci, L. De Stefano, I. Ruggiero, M. Terracciano, P. Dardano, N. Migliaccio, P. Arcari, R. Taté, I. Rendina and A. Lamberti, Diatomite biosilica nanocarriers for siRNA transport inside cancer cells. *Biochim. Biophys. Acta*, 2014, 1840, 3393–3403.

[32] N. Nassif, J. Livage, From diatoms to silica-based biohybrids. *Chem. Soc. Rev.*, 2011, 40, 849–859.

[33] M. De Stefano, L. De Stefano, Nanostructures in diatom frustules: functional morphology of valvocopulae in Cocconeidacean monoraphid taxa. *J. Nanosci. Nanotechnol.*, 2005, 5, 15–24.

[34] O. Şan, R. Gören and C. Özgür, Purification of diatomite powder by acid leaching for use in fabrication of porous ceramics. *Int. J. Miner. Process.*, 2009, 93, 6–10.

[35] Y. Wang, J. Cai, Y. Jiang, X. Jiang and D. Zhang, Preparation of biosilica structures from frustules of diatoms and their applications: current state and perspectives. *Appl. Microbiol. Biotechnol.*, 2013, 97, 453–462.

[36] R. Goren, T. Baykara and M. Marsoglu, A study on the purification of diatomite in hydrochloric acid. *Scand. J. Met.*, 2002, 31, 115–119.

[37] R. Goren, T. Baykare and M. Marsoglu, Effects of purification and heat treatment on pore structure and composition of diatomite. *Br. Ceram. Trans.*, 2002, 101, 177.

[38] Q. Xiaohua, L. Mingzhu, C. Zhenbin and L. Rui, Preparation and properties of diatomite composite superabsorbent. *Polym. Adv. Technol.*, 2007, 18, 184–193.

[39] E. M, Bens and C. M. Drew, Diatomaceous Earth: Scanning Electron Microscope of 'Chromosorb P'. *Nature*, 1967, 216, 1046.

[40] M. J. Carter and I. D. Milton, An inexpensive and simple method for DNA purifications on silica particles. *Nucleic Acids Res.*, 1993, 21, 1044.

[41] M. A. M. Khraisheh, M. A. Al-Ghouti, S. J. Allen and M. N. Ahmad, Effect of OH and silanol groups in the removal of dyes from aqueous solution using diatomite. *Water Res.*, 2005, 39, 922–932.

[42] A. R. Parker and H. E. Townley, Biomimetics of photonic nanostructures. *Nat. Nanotechnol.*, 2007, 2, 347–353.

[43] F. Xu, Y. Wang, X. Wang, Y. Tang and P. Yang, A Novel Hierarchical Nanozeolite Composite as Sorbent for Protein Separation in Immobilized Metal-Ion Affinity Chromatography. *Adv. Mater.*, 2003, 15, 1751–1753.

[44] J. Kim, P. Seidler, L. S. Wan and C. Fill, Formation, structure, and reactivity of amino-terminated organic films on silicon substrates. *J. Colloid Interface Sci.*, 2009, 329, 114–119.

[45] L. De Stefano, A. Lamberti, L. Rotiroti and M. De Stefano, Interfacing the nanostructured biosilica microshells of the marine diatom Coscinodiscus wailesii with biological matter. *Acta Biomater.*, 2008, 4, 126–130.

[46] L. De Stefano, Rotiroti, M. De Stefano, A. Lamberti, S. Lettieri, A. Setaro and P. Maddalena, Marine diatoms as optical biosensors. *Biosens. Bioelectron.*, 2009, 24, 1580–1584.

[47] M. Bariana, M. S. Aw, M. Kurkuri and D. Losic, Tuning drug loading and release properties of diatom silica microparticles by surface modifications. *Int. J. Pharm.*, 2013, 443, 230–241.

[48] S. A. Love, M. A. Maurer-Jones, J. W. Thompson, Y. S. Lin and C. L. Haynes, Assessing nanoparticle toxicity. *Annu. Rev. Anal. Chem.*, 2012, 5, 181–205.

[49] Y. S. Lin and C. L. Haynes, Synthesis and Characterization of Biocompatible and Size-Tunable Multifunctional Porous Silica Nanoparticles. *Chem. Mater.*, 2009, 21, 3979–3986.

[50] R. E. Serda, J. Gu, J. C. Bhavane, X. W. Liu, C. Chiappini, P. Decuzzi and M. Ferrari, The association of silicon microparticles with endothelial cells in drug delivery to the vasculature. *Biomaterials*, 2009, 30, 2440–2448.

[51] R. E. Serda, B. Godin, E. Blanco, C. Chiappini and M. Ferrari, Multi-stage delivery nano-particle systems for therapeutic applications. *Biochim. Biophys. Acta*, 2011, 1810, 317–329.

[52] L. Aagaard and J. J. Rossi, RNAi therapeutics: principles, prospects and challenges. *Drug Deliv. Rev.*, 2007, 59, 75–86.

[53] K. Gavrilov and V. M. Saltzman, Therapeutic siRNA: principles, challenges, and strategies. *J. Biol. Med.*, 2012, 85, 187–200.

[54] K. A. Whitehead, R. Langer and D. G. Anderson, Knocking down barriers: advances in siRNA delivery. *Nat. Rev. Drug Discov.*, 2009, 8, 129–138.

[55] W. X. Mai and H. Meng, Mesoporous silica nanoparticles: A multifunctional nano therapeutic system. *Integr. Biol.*, 2013, 5, 19–28.

[56] F. Simeoni, M. C. Morris, F. Heitz and G. Divita, Insight into the mechanism of the peptide-based gene delivery system MPG: implications for delivery of siRNA into mammalian cells. *Nucleic Acids Res.*, 2003, 31, 2717–2724.

[57] S. W. Kim, N. Y. Kim, Y. B. Choi, S. H. Park and J. M. Yang, S. Shin, RNA interference in vitro and in vivo using an arginine peptide/siRNA complex system. *J. Control. Release*, 2010, 10, 335–343.

[58] Y. Nakamura, K. Kogure, S. Futaki and H. Harashima, Octaarginine-modified multi-functional envelope-type nano device for siRNA. *J. Control. Release*, 2007, 119, 360–367.

[59] A. M. Chen, M. Zhang, D. Wei, D. Stueber, O. Taratula, T. Minko and H. He, Co-delivery of Doxorubicin and Bcl-2 siRNA by Mesoporous Silica Nanoparticles Enhances the Efficacy of Chemotherapy in Multidrug-Resistant Cancer Cells. *Small*, 2009, 5, 2673–2677.

[60] M. A. Shahbazi, P. V. Almeida, E. Mäkilä, M. Kaasalainen, J. Salonen, J. Hirvonen and H. A. Santos, Augmented cellular trafficking and endosomal escape of porous silicon nanoparticles via zwitterionic bilayer polymer surface engineering. *Biomaterials*, 2014, 35, 7488–7500.

[61] H. Otsuka, Y. Nagasaki and K. Kataoka, PEGylated nanoparticles for biological and pharmaceutical applications. *Adv. Drug Deliv. Rev.*, 2012, 64, 246–255.

[62] Q. Gao, Y. Xu, D. Wu, Y. Sun and X. Li, pH-Responsive Drug Release from Polymer-Coated Mesoporous Silica Spheres. *J. Phys. Chem. C*, 2009, 113, 12753–12758.

[63] A. Verma, O. Uzun, Y. Hu, Y. Hu, H. S. Han, N. Watson, S. Chen, D. J. Irvine and F. Stellacci, Surface-structure-regulated cell-membrane penetration by monolayer-protected nanoparticles. *Nat. Mater.*, 2013, 12, 588–595.

[64] E. Koren and V. P. Torchilin, Cell-penetrating peptides: breaking through to the other side. *Trends Mol. Med.*, 2012, 18, 385–393.

[65] M. C. Shin, J. Zhang, K. A. Min, K. Lee, Y. Byun, A. E. David, H. He and V. C. Yang, Cell-penetrating peptides: Achievements and challenges in application for cancer treatment *J. Biomed. Mater. Res. A*, 2014, 102, 575–587.

[66] M. Terracciano, M. A. Shahbazi, A. Correia, I. Rea, A. Lamberti, L. De Stefano and H. A. Santos, Surface bioengineering of diatomite based nanovectors for efficient intra-cellular uptake and drug delivery. *Nanoscale*, 2015, 7, 20063–20074.

[67] Y. Z. Huang, Y. F. Jiang, J. X. Wang, M. C. Shin, Y. Byun, H. He, Y. Liang and V. C. Yang, Curb challenges of the "Trojan Horse" approach: smart strategies in achieving effective yet safe cell-penetrating peptide-based drug delivery. *Adv. Drug Deliv. Rev.*, 2013, 64, 1299–1315.

[68] E. T. Vandenberg, L. Bertilsson, B. Liedberg, K. Uvdal, R. Erlandsson, H. Elwing and I. Lundström, Structure of 3-Aminopropyl Triethoxy Silane on Slicon Oxide. *J. Colloid Interface Sci.*, 1991, 147, 103–118.

[69] G. Socrates (Ed). Infrared and Raman Characteristic Group Frequencies: Tables and Charts. John Wiley & Sons, 2004.

[70] D. Liu, H. Zhang, E. Mäkilä, J. Fan, B. Herranz-Blanco, C. F. Wang, R. Rosa, A. J. Ribeiro, J. Salonen, J. Hirvonen and H. A. Santos, Microfluidic assisted one-step fabrication of porous silicon@acetalated dextran nanocomposites for precisely controlled combina-tion chemotherapy. *Biomaterials*, 2015, 39, 249–259.

[71] D. Schaer, A. I. Alayash and P. W. Buehler, Gating the radical hemoglobin to macro-phages: the anti-inflammatory role of CD163, a scavenger receptor. *Antioxid. Redox Signal.*, 2007, 9, 991–999.

[72] T. Yu, A. Malugin and H. Ghandehari, Impact of Silica Nanoparticle Design on Cellular Toxicity and Hemolytic Activity. *ACS Nano*, 2011, 5, 5717–5728.

[73] M. A. Shahbazi, M. Hamidi, E. Mäkilä, H. Zhang, P. V. Almeida, M. Kaasalainen, J. J. Salonen, J. T. Hirvonen and H. A. Santos, The mechanisms of surface chemistry effects of mesoporous silicon nanoparticles on immunotoxicity and biocompatibility. *Biomaterials*, 2013, 34, 7776–7789.

[74] H. Wu, G. Liu, S. Zhang, J. Shi, L. Zhang, Y. Chen, F. Chena and H. Chen, Biocompat-ibility, MR imaging and targeted drug delivery of a rattle-type magnetic mesoporous silica nanosphere system conjugated with PEG and cancer-cell-specific ligands. *J. Mater. Chem.*, 2011, 21, 3037–3045.

[75] Z. Zhang, M. Zhang, S. Chen, T. A. Horbett, B. D. Ratner and S. Jiang, Blood compati-bility of surfaces with superlow protein adsorption. *Biomaterials*, 2008, 29, 4285–4291.

[76] D. Fischera, Y. Lib, B. Ahlemeyerc, J. Krieglsteinc and T. Kissela, In vitro cytotoxicity testing of polycations: influence of polymer structure on cell viability and hemolysis. *Biomaterials*, 2003, 24, 1121–1131.

[77] H. J. P. Ryser, A Membrane Effect of Basic Polymers dependent on Molecular Size. *Nature*, 1967, 215, 934–936.

[78] H. He, J. Ye, Y. Wang, Q. Liu, H. S. Chung, Y. M. Kwon, M. C. Shin, K. Lee and V. C., Yang, Cell-penetrating peptides meditated encapsulation of protein therapeutics into intact red blood cells and its application. *J. Control. Release*, 2014, 176, 123–132.

[79] E. Jin, B. Zhang, X. Sun, Z. Zhou, X. Ma, Q. Sun, J. Tang, Y. Shen, E. Van Kirk, W. J. Murdoch and M. Radosz, Acid-Active Cell-Penetrating Peptides for in Vivo Tumor-Targeted Drug Delivery. *J. Am. Chem. Soc.*, 2013, 135, 933–940.

[80] J. Jo, S. Hong, W. Y. Choi and D. R. Lee, Cell-penetrating peptide (CPP)-conjugated proteins is an efficient tool for manipulation of human mesenchymal stromal cells. *Sci. Rep.*, 2014, 4, 4378.

[81] L. Vasconcelos, F. Madani, P. Arukuusk, L. Pärnaste, A. Gräslund and Ü. Langel, Effects of cargo molecules on membrane perturbation caused by transportan10 based cell-penetrating peptides. *Biochim. Biophys. Acta*, 2014, 1838, 3118–3129.

[82] M. Zorko and Ü. Langel, Cell-penetrating peptides: mechanism and kinetics of cargo delivery. *Adv. Drug. Deliv. Rev.*, 2005, 57, 529–545.

[83] S. W. Jones, R. Christison, K. Bundell, C. J. Voyce, S. M. V. Brockbank, P. Newham, M. A Lindsay, Characterisation of cell-penetrating peptide-mediated peptide delivery. *Br. J. Pharmacol.*, 2005, 145, 1093–1102.

[84] L. B. Slobodkin, P. E. Bossert, Ecology and Classification of North American Freshwater Invertebrates. San Diego: Academic Press, 2001.

[85] R. E. Steele, Developmental signaling in Hydra: what does it take to build a "simple" animal? *Dev. Biol.*, 2002, 248, 199–219.

[86] D. A. Holdway, K. Lok, M. Semaan, The acute and chronic toxicity of cadmium and zinc to two hydra species. *Environ. Toxicol.*, 2001, 16, 557–565.

[87] M. Sakaguchi, A. Mizusina, Y. Kobayakawa, Structure, development, and maintenance of the nerve net of the body column in Hydra. *J. Comp. Neurol.*, 1996, 373, 41–54.

[88] B. Quinn, F. Gagné, C. Blaise, Hydra, a model system for environmental studies. *Int. J. Dev. Biol.*, 2012, 56, 613–625.

[89] A. Ambrosone, L. Mattera, V. Marchesano, A. Quarta, A. S. Susha, A. Tino, A. L. Rogach, C. Tortiglione, Mechanisms underlying toxicity induced by CdTe quantum dots determined in an invertebrate model organism. *Biomaterials* 2012, 33, 1991–2000.

[90] A. Ambrosone, M. R. Scotto Di Vettimo, M. A. Malvindi, M. Roopin, O. Levy, M. Marchesano, P. P. Pompa, C. Tortiglione, A. Tino, Impact of amorphous SiO2 nano-particles on a living organism: morphological, behavioral, and molecular biology implications. *Front. Bioeng. Biotechnol.*, 2014, 2, 00037.

[91] V. Marchesano, A. Ambrosone, J. Bartelmess, F. Strisciante, A. Tino, L. E. Echegoyen, C. Tortiglione, S. Giordani, Impact of Carbon Nano-Onions on Hydra vulgaris as a Model Organism for Nanoecotoxicology. *Nanomaterials*, 2015, 5,1331–1350.

[92] C. Tortiglione, A. Quarta, M. A., Malvindi, A. Tino, T. Pellegrino, Fluorescent nano-crystals reveal regulated portals of entry into and between the cells of Hydra. *Plos One*, 2009, 4, 7698.

[93] C. Tortiglione, A. Quarta, A. Tino, L. Manna, R. Cingolani, T. Pellegrino, Synthesis and Biological Assay of GSH Functionalized Fluorescent Quantum Dots for Staining Hydra vulgaris. *Bioconjug Chem.*, 2007, 18, 829–835.

[94] V. Marchesano, Y. Hernandez, W. Salvenmoser, A. Ambrosone, A. Tino, B. Hobmayer, J. M. de la Fuente, C. Tortiglione, Imaging Inward and Outward Trafficking of Gold Nanoparticles in Whole Animals. *ACS Nano*, 2013, 7, 2431–2442.

[95] O. K. Wilby, J. M. Tesh, The Hydra assay as an early screen for teratogenic potential. *Toxicol. In Vitro*, 1990, 4, 582–583.

[96] W. F. Loomis, H. M. Lenhoff, Growth and sexual differentiation of hydra in mass culture. *J. Exp. Zool.*, 1956, 132, 555–557.

[97] A. Ambrosone, C. Tortiglione, Methodological approaches for nanotoxicology using cnidarian models. *Toxicol. Mech. Methods*, 2013, 23, 207–16.